

Mutations in the *SPTLC1* Protein Cause Mitochondrial Structural Abnormalities and Endoplasmic Reticulum Stress in Lymphoblasts

Simon J. Myers,^{1,2,*} Chandra S. Malladi,^{2,3,*} Ryan A. Hyland,^{1,2} Tara Bautista,⁴ Ross Boadle,^{5,6} Phillip J. Robinson,⁷ and Garth A. Nicholson^{8,9}

Mutations in serine palmitoyltransferase long chain subunit 1 (*SPTLC1*) cause the typical length-dependent axonal degeneration hereditary sensory neuropathy type 1 (HSN1). Transmission electron microscopy studies on *SPTLC1* mutant lymphoblasts derived from patients revealed specific structural abnormalities of mitochondria. Swollen mitochondria with abnormal cristae were clustered around the nucleus, with some mitochondria being wrapped in rough endoplasmic reticulum (ER) membranes. Total mitochondrial counts revealed a significant change in mitochondrial numbers between healthy and diseased lymphocytes but did not reveal any change in length to width ratios nor were there any changes to cellular function. However, there was a notable change in ER homeostasis, as assessed using key ER stress markers, BiP and ERO1- α , displaying reduced protein expression. The observations suggest that *SPTLC1* mutations cause mitochondrial abnormalities and ER stress in HSN1 cells.

Introduction

HEREDITARY SENSORY NEUROPATHY TYPE 1 (HSN1) is the most common dominantly inherited form of hereditary sensory neuropathy in man. The disorder has an onset in late childhood, teenage, or early adult years and produces sensory loss, which may go unnoticed. Loss of protective sensation can lead to painless skin injuries and ulcerations progressing to osteomyelitis and limb amputations. Degeneration of distal motor axons occurs later in life with distal and later proximal limb weakness. Pathology shows early sensory and motor distal axonal degeneration and later loss of dorsal root ganglia and spinal motor neurons (Denny-Brown, 1952).

HSN1 mutations in the serine palmitoyltransferase long chain subunit 1 (*SPTLC1*), cysteine (133) to tyrosine and valine (144) to aspartic acid mutations (Dawkins *et al.*, 2001), may produce structural changes that can cause disease via abnormal protein interactions. Whether these *SPTLC1* mutations produce the HSN phenotype through loss of enzyme

activity is unclear. Dedov *et al.* (2004) and others (Bejaoui *et al.*, 2002) have demonstrated a loss of activity with the cysteine (133) to tryptophan variant of human *SPTLC1*, as the mutation is close to the active site of the enzyme (Dedov *et al.*, 2004). However, there are no changes in SPT products in mutant SPT lymphoblasts (Dedov *et al.*, 2004). The newly described glycine (387) to alanine variant of human *SPTLC1* (Verhoeven *et al.*, 2004) is distant from the active site and is unlikely to affect enzyme activity. Recent studies suggest that these mutations cause a deleterious gain of function with the production of toxic sphingolipids (Hornemann *et al.*, 2009). Patients suffering from HSN1 have an abundance of these toxic sphingolipids in their blood stream, reflecting the observations of cell culture work.

Mitochondria play an essential role in peripheral nerves and are implicated in some hereditary neuropathies (Niemann *et al.*, 2005; Pedrola *et al.*, 2005; Berger *et al.*, 2006). Mitochondria are transported down peripheral nerves and cluster under areas of high-energy use such as internodes. Mutations in mitofusin 2 produce the most common form of

¹Neuro-Cell Biology Laboratory, School of Science & Health, University of Western Sydney, Campbelltown, NSW, Australia.

²Molecular Medicine Research Group, University of Western Sydney, Campbelltown, NSW, Australia.

³Molecular Physiology Unit, School of Medicine, University of Western Sydney, Campbelltown, NSW, Australia.

⁴Florey Neuroscience Institute, University of Melbourne, Victoria, Australia.

⁵Electron Microscope Laboratory, Institute of Clinical Pathology and Medical Research, Westmead, NSW, Australia.

⁶Westmead Millennium Institute, Westmead, NSW, Australia.

⁷Cell Signalling Unit, Children's Medical Research Institute, University of Sydney, Westmead, NSW, Australia.

⁸Northcott Neuroscience Laboratory, ANZAC Research Institute, University of Sydney, Concord, NSW, Australia.

⁹Molecular Medicine Laboratory, Concord Hospital, University of Sydney, Concord, NSW, Australia.

*These authors contributed equally to this work.

axonal Charcot-Marie-Tooth neuropathy (CMT type 2), and CMT VI with optic atrophy. Mutations in mitofusin 2 disrupt mitochondrial fusion (Legros *et al.*, 2002) and mitochondrial axonal transport (Baloh *et al.*, 2007). This is a length-dependent axonal neuropathy where the longest axons are affected first, commencing in the distal lower limbs and then in the distal upper limbs. Since mitochondrial transport is essential for distal axonal function, mitochondrial abnormalities have been proposed as the cause of a number of length-dependent or “dying back” hereditary neuropathies.

Since structural abnormalities have been found in neuropathies, we examined mitochondrial morphology, mitochondrial number, mitochondrial length-to-width ratio, polarity of mitochondrial membrane, and total cellular ATP levels in lymphoblasts expressing the HSN1 mutation in *SPTLC1*. We also monitored the expression of common ER stress markers and measured receptor-mediated endocytosis. We propose that cells expressing the *SPTLC1* mutations have mitochondrial structure abnormalities and a disrupted “ER homeostasis.”

Methods

Cell culture

Control and patient lymphoblasts (harboring C133W or V144D *SPTLC1* mutations) were maintained in 5% CO₂ and at 37°C in RPMI-1640 (Gibco BRL) plus 10% fetal calf serum (Gibco BRL), penicillin (100 µg/mL)/streptomycin (100 units/mL) (Sigma-Aldrich), and 2 mM L-glutamine (Sigma-Aldrich).

Electron microscopy

Control and *SPTLC1* mutant lymphoblasts were washed thrice before fixation in a modified Karnovsky fixative and washed in 0.1 M 3-(4-morpholino) propane sulfonic acid (MOPS) buffer (pH 7.4). After washing, the cells were postfixated in buffered 2% osmium tetroxide and dehydrated in an ethanol series before embedding in Spurr epoxy resin. Once polymerized (70°C for 10 h), sections were cut at 70 nm, stained with uranyl acetate and Reynold’s lead citrate and the sections were examined in a Philips CM120 BioTWIN electron microscope at 100 kV.

Indirect immunofluorescence and confocal microscopy

Lymphoblasts (1×10^6 cells) were suspended in 1 mL of warm phosphate-buffered saline (PBS). After centrifugation at 500 *g* for 5 min, the cell suspension was resuspended in 4% paraformaldehyde containing 0.3% Triton X-100 and incubated at 37°C for 30 min. The cells were then centrifuged and blocked in 1% bovine serum albumin solution at 37°C for 30 min. After washing, the cells were resuspended in primary antibody, MTCO2 (Abcam, 1:50), and incubated for 1 h at room temperature. The cells were washed and resuspended in secondary antibody, anti-mouse Rhodamine (Millipore; 1:200), and incubated for 1 h at room temperature. DAPI stain (1 µg/µL) was added to the cell suspension and after 2 min, the cells were centrifuged and washed twice. Aliquots (200 µL) were added to microtiter plate wells containing coverslips coated in Histogrip. The coverslips were washed in warm PBS, left overnight to dry, and mounted onto glass slides before confocal imaging using Zeiss Zen 2009.

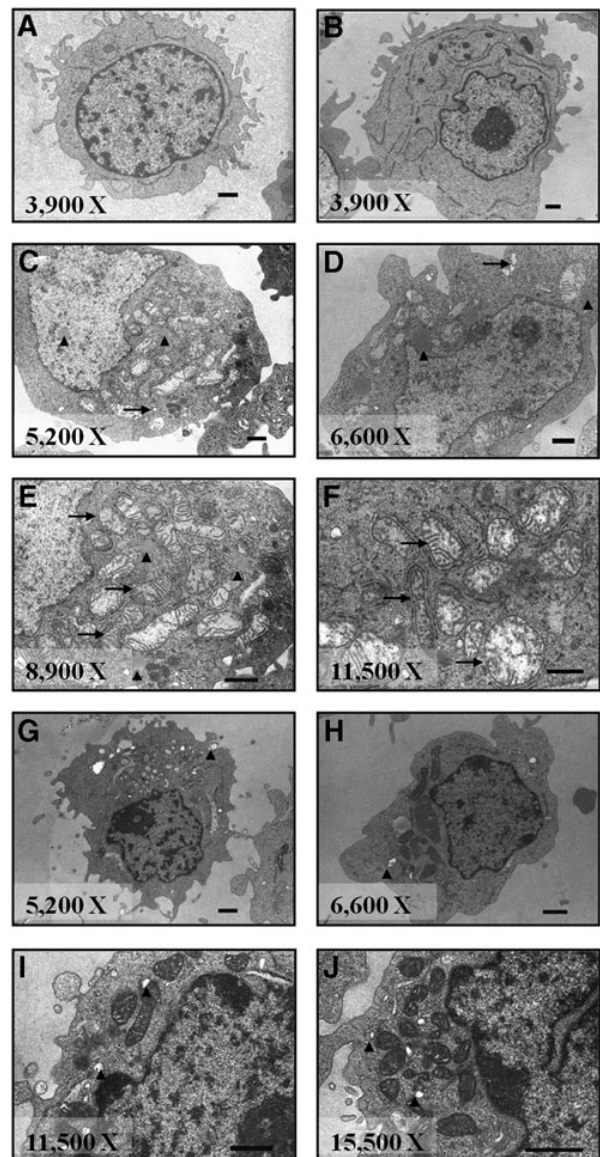


FIG. 1. Representative transmission electron micrographs (TEM) of cells from two different cultures of control and serine palmitoyltransferase long chain subunit 1 (*SPTLC1*) mutant lymphoblasts. (**A, B**) Control lymphoblasts displaying typical large nuclei and mitochondria. In *SPTLC1* mutant lymphoblasts expressing the C133W mutations; lipid droplets (arrowheads) and vacuole structures (arrows) are observed as well as peri-nuclear localization of the mitochondria (**C, D**), the endoplasmic reticulum (arrows) is also seen to be tightly wrapped around the mitochondria (**E, F**). In *SPTLC1* mutant lymphoblasts expressing the V144D mutations; multi-vesicular bodies (arrowheads) are present as well as peri-nuclear localization of the mitochondria (**G–J**). Scale bars 2 µm.

Flow cytometry

Aliquots of each cell suspension (40 µL) from section 2.3 were analyzed using the MACSquant flow cytometer (Miltenyi Biotech) and analyzed with MACSquant software. Live

single cells were gated, and the mean of fluorescence was obtained per 10,000 events.

Mitoprobe JC-1 assay (mitochondrial membrane potential)

Lymphoblasts (1×10^6 cells) were suspended in 1 mL of warm PBS. Carbonyl cyanide 3-chlorophenylhydrazone (CCCP; membrane uncoupler) (50 mM, 1 μ L) was added to the control tube and incubated at 37°C for 5 min. JC-1 (2 μ M) was added to all the cells, and the cells were incubated at 37°C, 5% CO₂ for 30 min. Cells were washed once in PBS (2 mL), and then pelleted by centrifugation. PBS (500 μ L) was added to each tube, and samples were analyzed by flow cytometry (BD FACScan) with 488 nm excitation, where the depolarized mitochondria fluoresce green.

Annexin V apoptosis assay

As per the manufacturer's instructions (BD Biosciences Pharmingen) briefly, lymphoblasts (1×10^6 cells/mL) were washed twice in cold PBS and resuspended in 1 \times binding buffer. About 1×10^5 cells (in 100 μ L) were transferred to a 5 mL culture tube, where 5 μ L of Annexin V-FITC and 5 μ L

of Propidium Iodide was added. Cells were gently vortexed and incubated at room temperature for 15 min in the dark. Binding buffer (1 \times , 400 μ L) was added to each tube, and samples were analyzed by flow cytometry (BD FACScan).

Cellular ATP assay

The total cellular ATP level of the lymphoblasts was measured using the ATPlite luminescence ATP detection assay system kit (Perkin Elmer) according to the manufacturer's instructions. Plates were dark adapted for 10 min, and luminescence was measured using the luminometer (Victor 3 Multi Label Reader; Perkin Elmer).

Clathrin-mediated endocytosis assay

Lymphoblasts from healthy donors and from patients affected with HSN1 were cultured in RPMI that was supplemented with 10% FBS, 2% glutamine for 4 days. Clathrin-mediated endocytosis (CME) was performed after 24 h serum starvation in RPMI medium. Briefly, cells were incubated in a 5% CO₂ incubator with Alexa Fluor 594 conjugated transferrin (Molecular Probes) for 10 min and immediately washed with acetic acid (0.2 M) with NaCl (0.5 M) for 10 min on ice. After acid wash, cells were fixed in 4% p-formaldehyde for 10 min

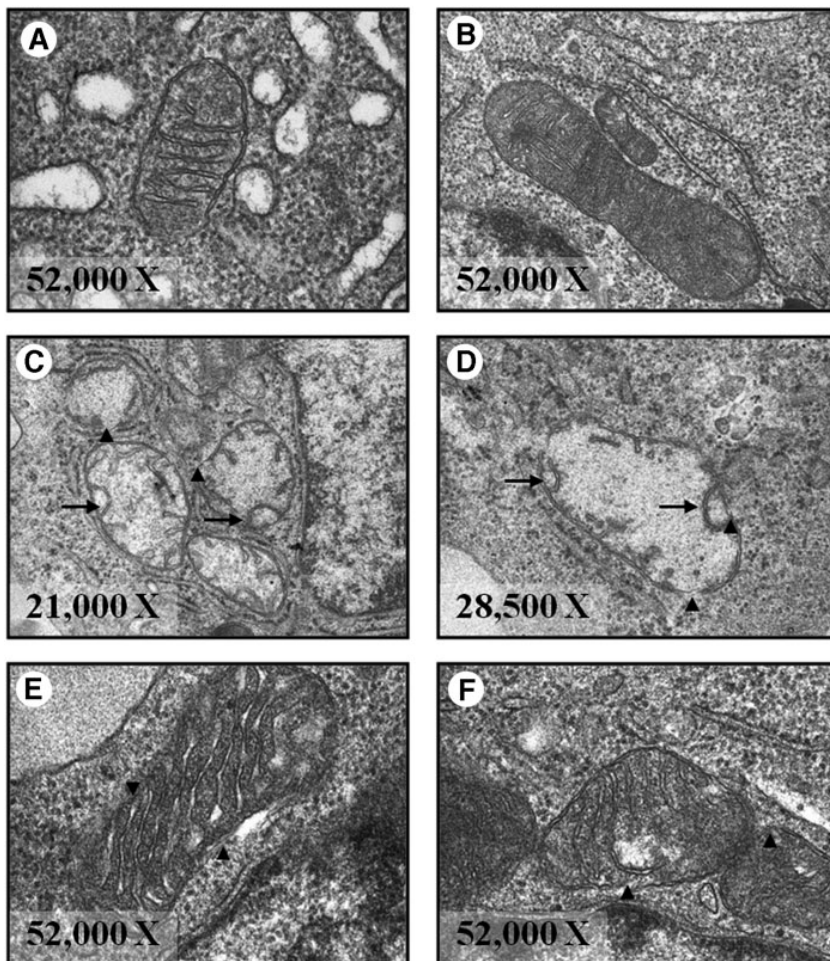


FIG. 2. Representative TEM displaying mutation specific ultrastructural changes from two different cultures of *SPTLC1* mutant lymphoblasts. Control lymphoblasts at 31,500 magnification show a continuous outer membrane with no breakages and are of normal size (A, B). In *SPTLC1* mutant lymphoblasts expressing the C133W mutations; display a discontinuous outer membrane and sections where there is complete breakage of the membrane (arrowheads) (C, D). Arrows denote a curved membrane, which appears to bridge the breakage. In *SPTLC1* mutant lymphoblasts expressing the V144D mutations; display electron dense and grossly swollen cristae along with discontinuous outer membranes (arrowheads) (E, F).

at room temperature. Cells were washed with cold PBS, and the nucleus was stained with DAPI. Both control and patient cells were spun on microscope slides ($5 \times 75 \times 1$ mm Menzel-Glasser Super Frost plus; CE Invitro Diagnostics) using Shandon Cytospin 4 (Thermo) at 800rpm for 2min. Transferrin uptake was measured in lymphoblasts and COS-7 cells using MetaMorph Offline ver.6.2r1 software.

Western blots

Protein extracts (20 μ g) from each lymphoblast sample were electrophoresed on a 12.5% sodium dodecyl sulfate polyacrylamide gel electrophoresis gels, transferred to polyvinylidene difluoride (0.2 μ m) membranes, and probed using the following antibodies: mouse anti-MTCO2 (Abcam; 1:2000), mouse anti-Actin (Millipore; 1:2,000,000), and rabbit anti-BiP (Cell Signaling; 1:1000). Western blots were developed using chemiluminescence and imaged using the AGFA CP1000 X-ray processor (AGFA) followed by analysis with Image-J by densitometry.

Results

Structural changes to mitochondrial morphology in SPTLC1 mutant lymphoblasts

To observe the effect of the SPTLC1 mutations on cellular morphology, transmission electron microscopy (TEM) was performed on control and SPTLC1 mutant lymphoblasts containing either the C133W or the V144D mutation. Gross disruption of mitochondrial morphology was apparent (Fig. 1). Control lymphoblasts display normal mitochondrial morphology and normal structure (Fig. 1A, B). Lymphoblasts carrying the C133W mutation have numerous lipid droplet deposits (arrowheads), vacuolar structures (arrows) and there appears to be reduced membrane ruffles in these cells (Fig. 1C, D). At a higher magnification, the perinuclear-clustered mitochondria are “wrapped” in rough endoplasmic reticulum (RER) in the cells expressing this C133W mutation (arrows) (Fig. 1E, F). In cells containing the V144D mutation, the membrane surface displays reduced ruffling as compared with control cells. There are vacuolar inclusions and the appearance

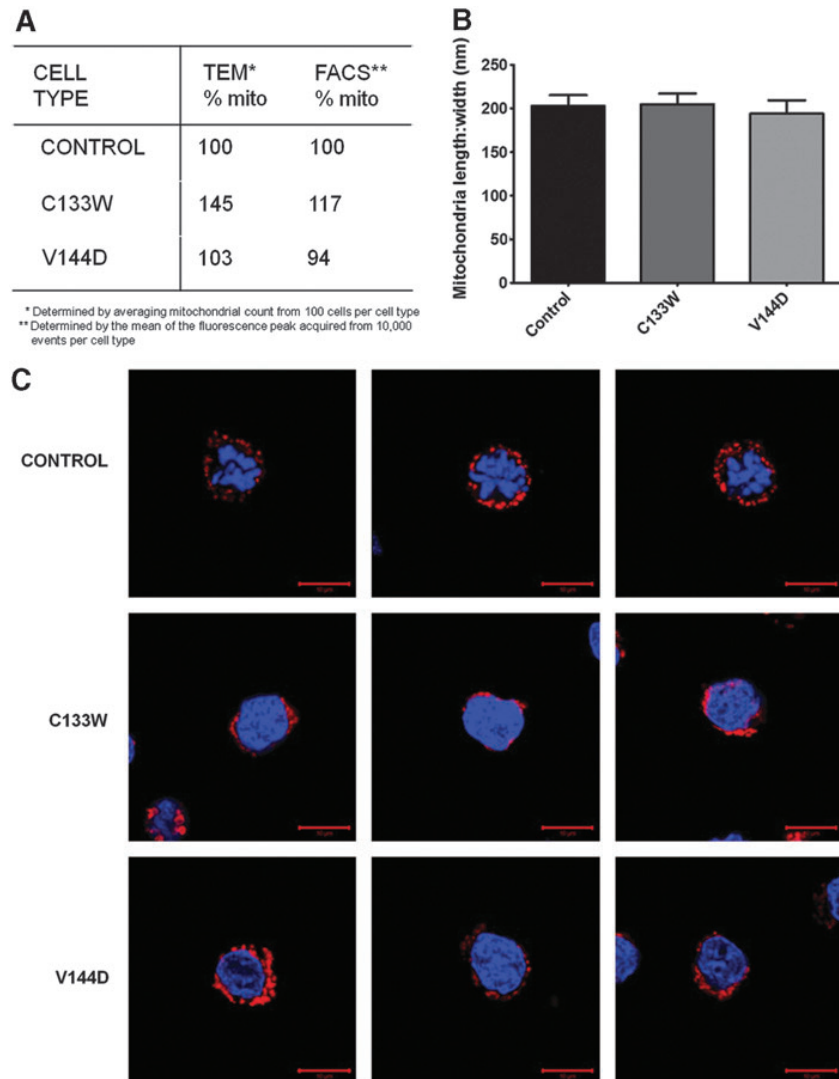


FIG. 3. Total mitochondrial numbers and mitochondrial length/width ratios. **(A)** % mitochondrial numbers per cell was determined by TEM (average of 100 cells) and flow cytometry (MTCO2 stained cells, mean of fluorescence peak from 10,000 events). **(B)** Length-to-width ratios of the mitochondria counted in **(A)** ($n = 100, \pm$ SD). **(C)** Immunofluorescence of cells stained with MTCO2 (Red), and Dapi (Blue).

of multi-vesicular bodies (MVBs; denoted by arrowheads, Fig. 1G–J). The morphology-challenged mitochondria appear to be peri-nuclear localized in the lymphoblasts carrying the C133W mutation.

Figure 2A and B displays mitochondria in isolation from control lymphoblasts that show a continuous outer membrane with no breakages, and they appear of normal size and are not excessively electron dense. In cells expressing the C133W SPTLC1 mutation, there is a discontinuous outer mitochondrial membrane and areas of complete membrane breakage (arrowheads) (Fig. 2C, D). In addition, arcs of cristae membrane appear to form where full mitochondrial membrane breakage occurs (arrows). In cells carrying the V144D SPTLC1 mutation, disturbance to the continuity of the outer mitochondrial membrane is also observed (arrowheads) (Fig. 2E, F). However, the major morphological findings with this mutation are that the mitochondria are extremely electron dense and have grossly enlarged cristae.

Total mitochondrial numbers in SPTLC1 mutant lymphoblasts

Due to the change in structure and localization of mitochondria in cells expressing the SPTLC1 mutations, total mitochondrial number and length-to-width ratios were determined. Figure 3A displays total mitochondrial counts as determined by TEM and flow cytometry, with each number representing the % number of mitochondria per cell taken from 100 cells or 10,000 cells respectively. The C133W mutation in SPTLC1 increases mitochondrial number, but this is not observed in the V144D mutation. Mitochondrial length-to-width ratios revealed no difference between control and mutant SPTLC1 cells (Fig. 3B). Indirect immunofluorescence detection of the mitochondria-specific marker MTCO2 (red) displayed no change to the cellular localization of the mitochondria between control and mutant SPTLC1 cells (Fig. 3C).

Mitochondrial membrane potential in nonapoptotic SPTLC1 mutant lymphoblasts

In order to determine whether the morphological changes to the inner and outer mitochondrial membranes affect mitochondrial membrane potential a JC-1 assay was performed. Figure 4A shows a graphical representation of polarized versus nonpolarized mitochondria measured as a percentage of cellular events from compiled flow cytometry scans. These data show normal mitochondrial membrane potential for control lymphoblasts (open bars) with drug-induced (CCCP) depolarization of mitochondrial membranes in control cells (negative control) displaying complete mitochondrial membrane uncoupling. However, in the overall pooled data from the SPTLC1 mutant lymphoblasts, there was a small but not a significant increase in membrane depolarization (shaded bars). To determine whether this slight increase in mitochondrial membrane depolarization affected the overall ATP content in the patient cells, total ATP levels were assayed. There was no significant difference between control (open bars) and patient (hatched bars) samples (Fig. 4B). To confirm that the cells were not actively undergoing apoptosis, the Annexin V assay was performed. A histogram of control (open bars) and patient (solid bars) lymphoblast cells shows that the cells were not apoptotic (Fig. 4C).

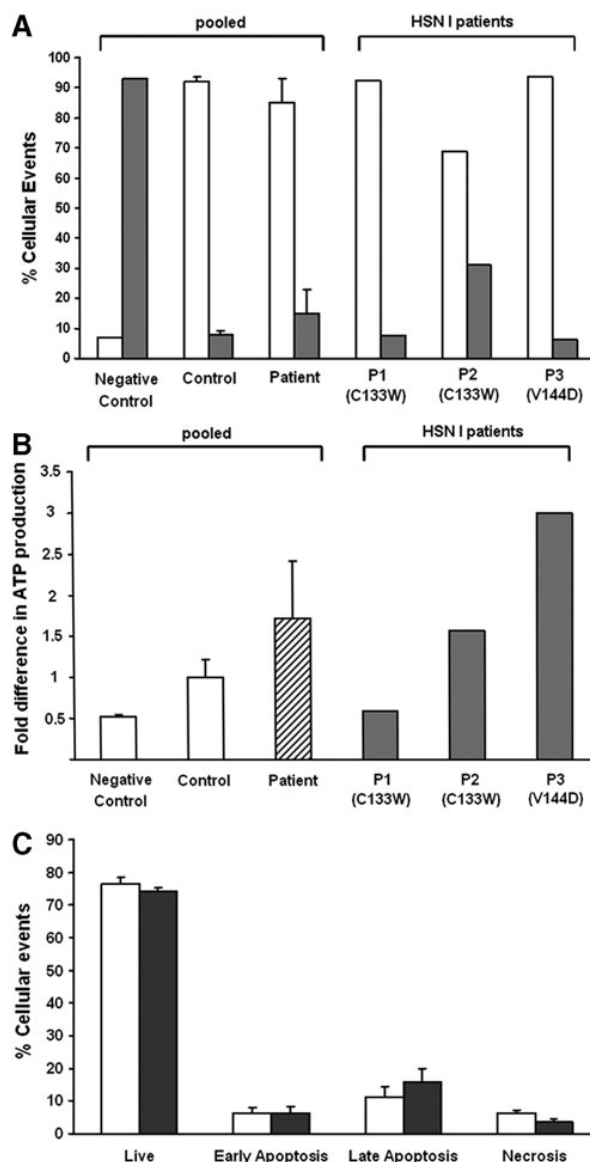


FIG. 4. Intracellular energy levels and apoptosis profile in SPTLC1 mutant lymphoblasts. **(A)** Mitochondrial membrane potential was measured in SPTLC1 mutant lymphoblasts using the Mitoprobe JC-1 assay kit for flow cytometry. Data are represented as a percentage of polarized mitochondria (open bars) to depolarized mitochondria (solid bars) in a pooled population ($n=3$) and in individual patients ($n=1$ but performed in triplicate). For each sample $n=3, \pm$ SD. **(B)** ATP levels were assayed in control and SPTLC1 mutant lymphoblasts using the ATPlite luminescence ATP detection kit (Perkin-Elmer). Data are represented as a fold change in ATP production where the control cells are in open bars ($n=3$) and the pooled patient cells are hatched bars ($n=3$). For each sample $n=3, \pm$ SD. The individual patient cells are displayed in solid bars ($n=1$ but performed in triplicate). **(C)** The results of an Annexin V assay where the data are shown as a percentage of cellular events for a pooled population of control (open bars) ($n=3$) and patient (solid bars) ($n=3$) samples. Live cell, early apoptotic, late apoptotic, and necrotic cell populations are exhibited. For each sample $n=3, \pm$ SD.

Endocytosis in SPTLC1 mutant lymphoblasts

To determine whether the morphologically challenged mitochondria affected other energy utilizing cellular events, CME was assayed by the observed uptake of fluorescent labeled transferrin into the cell. The same amount of transferrin (red) uptake was observed for control, C133W, and V144D lymphoblasts (Fig. 5A–C). Single cell analysis shows no variation in CME between control cells (Fig. 5D–G) and C133W (Fig. 5H–K) and V144D (Fig. 5L–O) mutant cells. Cells were counter-stained with the nuclear stain DAPI to display the nucleus and show the localization of transferrin-filled endosomes. Quantitative analysis revealed no statistical difference in CME between the three cell types (Fig. 5P).

Disruption to ER homeostasis in SPTLC1 mutant lymphoblasts

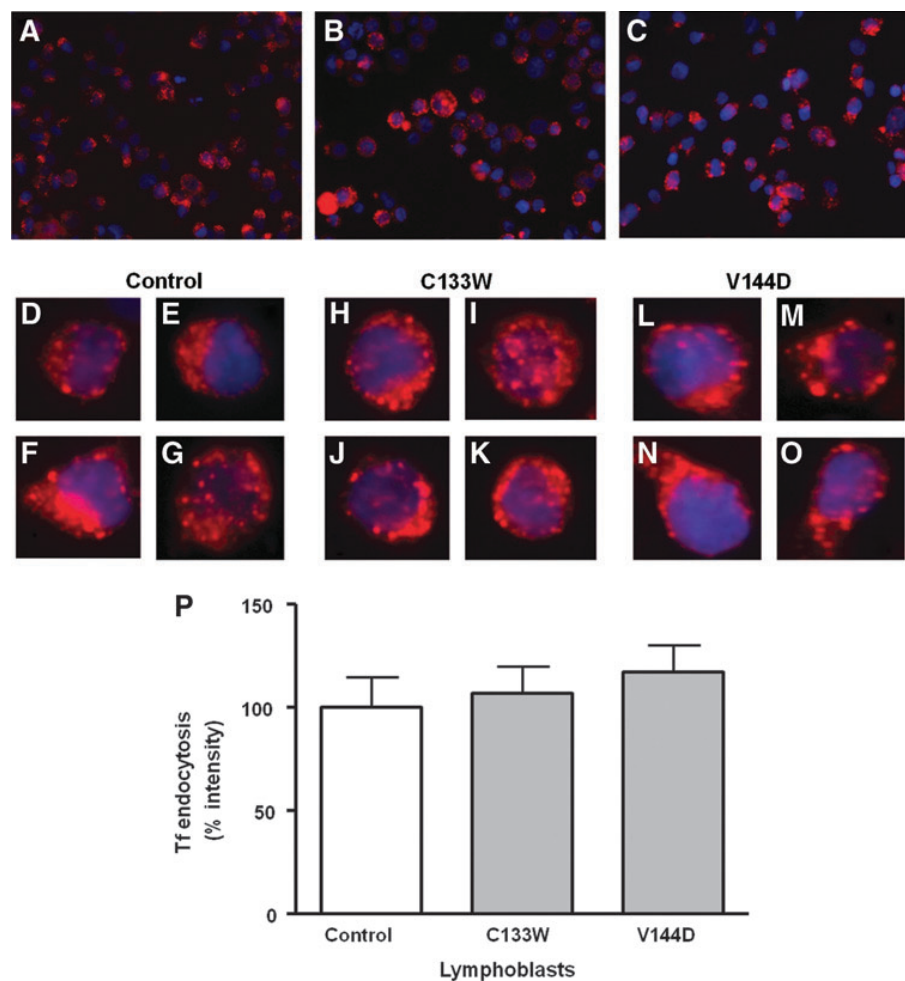
As observed in TEMs (Fig. 1), the dysfunctional mitochondria in the C133W mutant SPTLC1 patient cells are wrapped in RER. Since the SPTLC1 protein is located in the ER, we determined whether there is a changed expression of ER stress marker proteins associated with these mutants (Fig. 6). MTCO2, a marker for mitochondria, is unchanged in these mutant cells (Fig. 6A, B). Interestingly, there was a

significant increase in actin protein expression levels in mutant SPTLC1 cells (Fig. 6A, C). In cells expressing the C133W and V144D mutation in SPTLC1, BiP expression levels significantly decreased and were almost undetectable in V144D cells (Fig. 6A, D). A significant decrease was also seen in ERO1- $L\alpha$, which is responsible for maintaining the reduction potential of the ER (Fig. 6A, E).

Discussion

Our data indicate that the SPTLC1 mutations disrupt mitochondrial morphology in lymphoblasts, by which the ER wraps tightly around the mitochondria and ER stress appears to be induced. Minimal loss of mitochondrial charge is associated with the dysfunctional mitochondria. The mechanism by which this process is occurring is unknown. However, the apparent increase in stress due to SPTLC1 mutations may also make use of the mitochondria-ER membrane juxtaposition (Martins de Brito and Scorrano, 2010), leading to a collaboration between the mitochondria and the ER for lipid exchange proteins to be transferred across the organelles via the mitochondrial-associated membrane (MAM) space and to dysregulate calcium efflux to the mitochondria (Fig. 7).

FIG. 5. Endocytosis in SPTLC1 mutant lymphoblasts. Hereditary sensory neuropathy type 1 (HSN1) lymphoblasts have normal receptor-mediated endocytosis (RME) function. (A–C) Full-field views of control cells, C133W, and V144D patient lymphoblasts (respectively) where the nucleus has been stained with DAPI (blue), and CME was measured by the uptake of fluorescent-labeled transferrin (red). (D–G) Single cell images of control lymphoblasts; (H–K) single cell images of C133W patient lymphoblasts and (L–O) single cell images of V144D patient lymphoblasts, all showing normal uptake of transferrin (red) and the nucleus is stain with DAPI (blue). (P) A graphical representation of transferrin uptake measured as a percentage intensity of control, C133W patient, and V144D patient lymphoblasts ($n = 400$ cells per group).



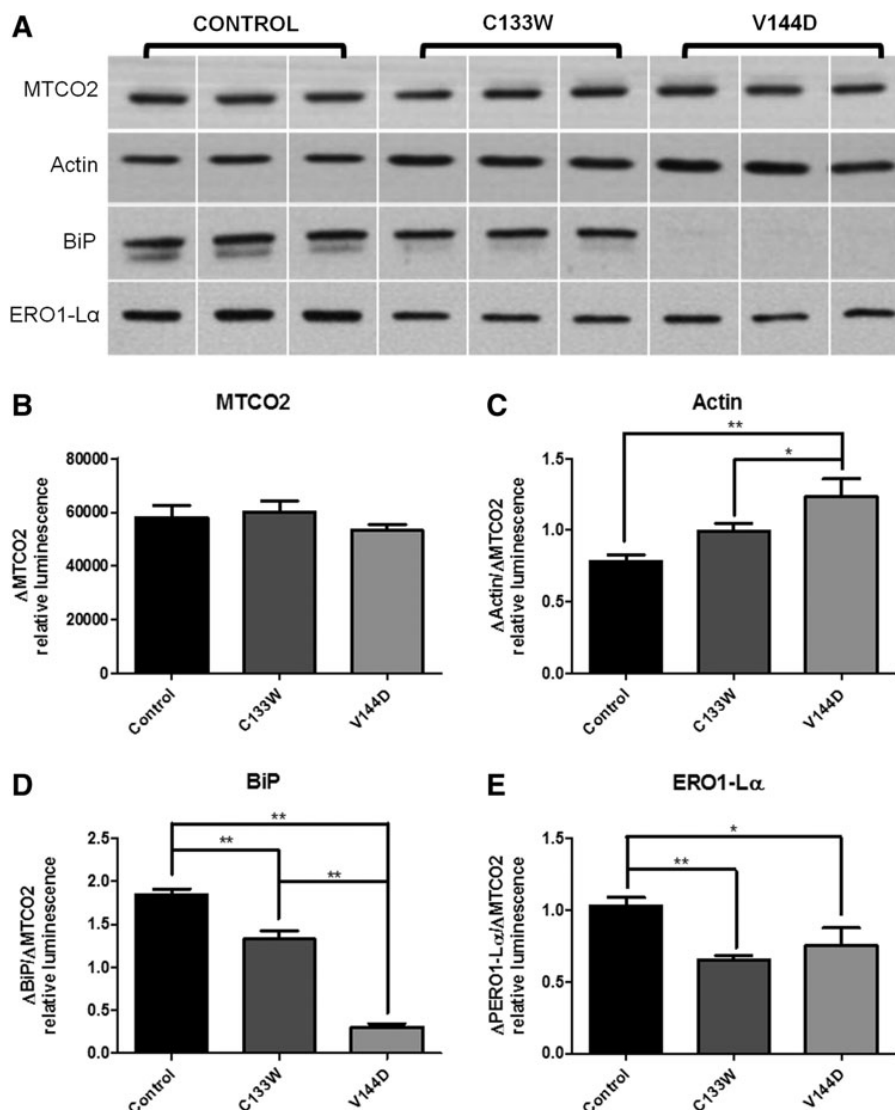


FIG. 6. Protein expression levels of several markers in SPTLC1 mutant lymphoblasts. **(A)** Western blot results of MTCO2: a mitochondrial marker, actin: key component of the cytoskeleton, BiP: the key regulator in protein folding and endoplasmic reticulum (ER) stress and ERO1-L α ; responsible for maintaining the redox balance within the ER. **(B)** The raw luminescence data for MTCO2 ($n=3, \pm SD$). **(C-E)** The normalized data for actin, BiP, and ERO1-L α , respectively ($n=3, \pm SD$). * $p > 0.05$, ** $p > 0.01$.

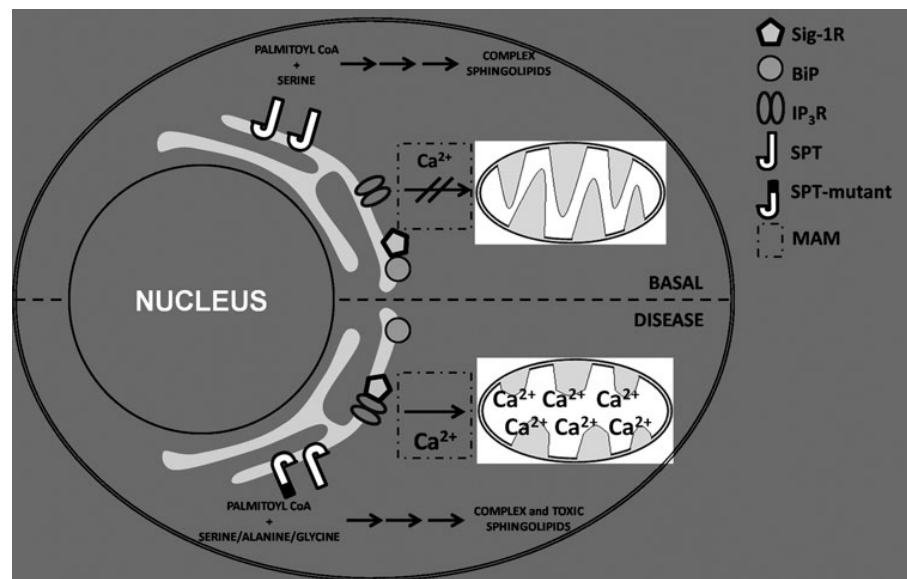
The link between SPTLC1 mutations and the observed mitochondrial changes is yet to be explored. The apposition of the ER to mitochondria suggests a direct link (Martins de Brito and Scorrano, 2010). In general, decreasing the space between the ER and mitochondria will cause an increase in the concentration of Ca^{2+} within the MAM space, thus elevating mitochondrial Ca^{2+} levels. If one considers the dual function of ER chaperone immunoglobulin heavy-chain binding protein (BiP), first as a molecular chaperone and inhibitor of the ER stress response, and second as an inhibitor of Ca^{2+} flux through the ER to the mitochondria through Sigma-1 receptor and inositol trisphosphate receptor, then it is likely that small changes in BiP expression levels could lead to large detrimental effects in mitochondrial form, as observed in the C133W SPTLC1 mutant, and function. The observation in the V144D SPTLC1 mutant that BiP expression is down-regulated offers another mechanism of action, suggesting that this mutation may negatively regulate the molecular pathway associated with

BiP. This possibly provides a functional link between ER homeostasis and mitochondrial structure and function.

This is the first time that such a study has been performed on HSN1 cells which show these ultrastructural changes to mitochondria. In a yet-to-be-published study from our laboratory, other CMT types caused by mutations in mitofusin 2 and in dynamin 2 appear to present with different ultrastructural changes than those observed in these HSN1 cells caused by the SPTLC1 mutations. In a study conducted by Parra *et al.*, (2008), it was shown that ceramide induces a loss of mitochondrial connectivity and mitochondrial fragmentation, ultimately leading to apoptosis; this finding was in direct contrast to our studies that exhibit no apoptosis.

Functional mitochondria are usually transported along microtubules, with depolarized mitochondria returning to the perinuclear region of the cell, suggesting that partially depolarized mitochondria may not be transported distally (Baloh *et al.*, 2007). Therefore, a minimal loss in mitochondrial charge may be sufficient to disrupt mitochondrial

FIG. 7. A schematic representation of findings observed in this study showing the liaison between the mitochondria, ER, calcium, and SPTLC1.



transport, especially if extrapolated to the long distances involved in a sensory neuron. Failure of the damaged mitochondria to reach the periphery may lead to changes in the distal axon, which may cause axonal degeneration. The precise degeneration mechanism is unknown but may make use of normal developmental processes, such as retraction or autophagy/mitophagy. These mitochondrial changes do not appear to affect cellular apoptosis and obviously do not affect CME in these cells. Likewise, they do not support an active mitophagy process, as mitochondrial membrane potential would have been affected with depolarization of the mitochondria (Min Jin and Youle, 2012). Ultrastructural analysis should have displayed multi-lamellar (like) bodies where the individual dysfunctional mitochondria have been continuously wrapped in ER membrane or have engulfed the ER membrane (Min Jin and Youle, 2012).

It is possible that the mutant SPTLC1 protein interferes with the delivery of essential proteins, lipid, or Ca^{2+} from the ER to the mitochondria (Bereiter and Voth, 1994; Wang *et al.*, 2007). The significant decrease in BiP and ERO1-L α protein expression in SPTLC1 mutants suggests that ER stress may play a role in this disease. Since BiP is the key regulator of protein folding and cellular responses to ER stress, we suggest that the mutants have an affected ER homeostasis which could lead to an abnormal interaction between the ER and mitochondria. Whether this is related to Ca^{2+} flux through the cell is unknown.

Both the ER and mitochondria bind to microtubules and actin filaments, using the cytoskeleton as scaffolding for shape and localization. The change in actin protein expression may help explain the close proximity of the ER to the mitochondria through a change in the stabilization points between the two organelles (Sturmer *et al.*, 1995). The change in actin is also important, as it may explain axonal degeneration in sensory neurons carrying the SPTLC1 mutation through the inability of mitochondria to migrate to the terminal end of the axon. An understanding of this process may lead to therapeutic strategies, which may correct the

mitochondrial defect and, therefore, arrest the axonal degeneration found in this disease.

All of the hereditary neuropathies produce disability through the common feature of axonal degeneration (Sahenk, 1999). Even initial demyelinating forms of neuropathy eventually result in axonal degeneration (Madrid *et al.*, 1977). This is thought to be the result of disturbed Schwann cell and axonal interactions and possibly the spread of high-conductance sodium channels (Custer *et al.*, 2003). Although much is known about the cell biology of many of the neuropathy genes, little is known about how they promote axonal degeneration in neurons.

This study provides evidence that SPTLC1 mutations cause mitochondrial abnormalities and ER stress in cells derived from patients. In other studies investigating hereditary neuropathies, mitochondrial abnormalities have been suggested to be the causal mechanism (Abu-Amero and Bosley, 2006; Kwong *et al.*, 2006; Misaka *et al.*, 2006; Baloh *et al.*, 2007), adding to the discussion that there is potentially a mitochondrial trafficking defect within these cells. How these changes cause distal axonal degeneration is poorly understood. Various mechanisms have been proposed; one suggestion is the process of “localized apoptosis” (Carson *et al.*, 2005). Here for the first time, we show that cells expressing the SPTLC1 mutations have mitochondrial structure abnormalities and disrupted “ER homeostasis,” revealing a link between mitochondria, ER, lipids, and calcium by which a common molecular mechanism appears close to being elucidated.

Acknowledgments

This work was supported in part by research grants from USA-MDA (to G.N. and S.M.) and NH&MRC of Australia (to P.J.R. and G.N.).

Disclosure Statement

No competing financial interests exist.

References

- Abu-Amero, K.K., and Bosley, T.M. (2006). Mitochondrial abnormalities in patients with LHON-like optic neuropathies. *Invest Ophthalmol Vis Sci* **47**, 4211–4220.
- Baloh, R.H., Schmidt, R.E., Pestronk, A., and Milbrandt, J. (2007). Altered axonal mitochondrial transport in the pathogenesis of Charcot-Marie-Tooth disease from mitofusin 2 mutations. *J Neurosci* **27**, 422–430.
- Bejaoui, K., Uchida, Y., Yasuda, S., Ho, M., Nishijima, M., Brown, R.H. Jr., Holleran, W.M., and Hanada, K. (2002). Hereditary sensory neuropathy type I mutations confer dominant negative effects on serine palmitoyltransferase, critical for sphingolipid synthesis. *J Clin Invest* **110**, 1301–1308.
- Bereiter-Hahn, J., and Voth, M. (1994). Dynamics of mitochondria in living cells: shape changes, dislocations, fusion and fission of mitochondria. *Microscopy Res Tech* **27**, 198–219.
- Berger, P., Niemann, A., and Suter, U. (2006). Schwann cells and the pathogenesis of inherited motor and sensory neuropathies (Charcot-Marie-Tooth disease). *Glia* **54**, 243–257.
- Carson, C., Saleh, M., Fung, F.W., Nicholson, D.W., and Roskams, A.J. (2005). Axonal dynactin p150glued transports caspase-8 to drive retrograde olfactory receptor neuron apoptosis. *J Neurosci* **25**, 6092–6104.
- Custer, A.W., Kazarinova-Noyes, K., Sakurai, T., Xu, X., Simon, W., Grumet, M., and Shrager, P. (2003). The role of the ankyrin-binding protein NrCAM in node of Ranvier formation. *J Neurosci* **23**, 10032–10039.
- Dawkins, J.L., Hulme, D.J., Brahmbhatt, S.B., Auer-Grumbach, M., and Nicholson, G.A. (2001). Mutations in SPTLC1, encoding serine palmitoyltransferase, long chain base subunit-1, cause hereditary sensory neuropathy type I. *Nat Gen* **27**, 309–312.
- Dedov, V.N., Dedova, I.V., Merrill, A.H. Jr., and Nicholson, G.A. (2004). Activity of partially inhibited serine palmitoyltransferase is sufficient for normal sphingolipid metabolism and viability of HSN1 patient cells. *Biochim Biophys Acta* **1688**, 168–175.
- Denny-Brown, D. (1952). The nature of muscular diseases. *Can Med Assoc J* **67**, 1–6.
- Hornemann, T., Penno, A., Richard, S., Nicholson, G. van Dijk, F., Rothier, A., Timmerman, V., and von Eckardstein, A. (2009). A systematic comparison of all mutations in hereditary sensory neuropathy type I (HSAN I) reveals that the G387A mutation is not disease associated. *Neurogenetics* **10**, 135–143.
- Kwong, J.Q., Beal, M.F., and Manfredi, G. (2006). The role of mitochondria in inherited neurodegenerative diseases. *J Neurochem* **97**, 1659–1675.
- Legros, F., Lombes, A., Frachon, P., and Rojo, M. (2002). Mitochondrial fusion in human cells is efficient, requires the inner membrane potential, and is mediated by mitofusins. *Mol Biol Cell* **13**, 4343–4354.
- Madrid, R., Bradley, W.G., and Davis, C.J. (1977). The peroneal muscular atrophy syndrome. Clinical, genetic, electrophysiological and nerve biopsy studies. Part 2. Observations on pathological changes in sural nerve biopsies. *J Neurol Sci* **32**, 91–122.
- Martins de Brito, O., and Scorrano, L. (2010). An intimate liaison: spatial organization of the endoplasmic reticulum-mitochondria relationship. *EMBO J* **29**, 2715–2723.
- Min Jin, S., and Youle, R. (2012). PINK1- and Parkin- mediated mitophagy at a glance. *J Cell Sci* **125**, 795–799.
- Misaka, T., Murate, M., Fujimoto, K., and Kubo, Y. (2006). The dynamin-related mouse mitochondrial GTPase OPA1 alters the structure of the mitochondrial inner membrane when exogenously introduced into COS-7 cells. *Neurosci Res* **55**, 123–133.
- Niemann, A., Ruegg, M., La Padula, V., Schenone, A., and Suter, U. (2005). Ganglioside-induced differentiation associated protein 1 is a regulator of the mitochondrial network: new implications for Charcot-Marie-Tooth disease. *J Cell Biol* **170**, 1067–1078.
- Parra, V., Eisner, V., Chiong, M., Criollo, A., Moraga, F., Garcia, A., Hartel, S., Jaimovich, E., Zorzano, A., Hidalgo, C., and Lavandero, S. (2008). Changes in mitochondrial dynamics during ceramide-induced cardiomyocyte early apoptosis. *Cardiovasc Res* **77**, 387–397.
- Pedrola, L., Espert, A., Wu, X., Claramunt, R., Shy, M.E., and Palau, F. (2005). GDAP1, the protein causing Charcot-Marie-Tooth disease type 4A, is expressed in neurons and is associated with mitochondria. *Hum Mol Genet* **14**, 1087–1094.
- Sahenk, Z. (1999). Abnormal Schwann cell-axon interactions in CMT neuropathies. The effects of mutant Schwann cells on the axonal cytoskeleton and regeneration-associated myelination. *Ann NY Acad Sci* **883**, 415–426.
- Sturmer, K., Baumann, O., and Walz, B. (1995). Actin-dependent light-induced translocation of mitochondria and ER cisternae in the photoreceptor cells of the locust *Schistocerca gregaria*. *J Cell Sci* **108**, 2273–2283.
- Verhoeven, K., Coen, K., De Vriendt, E., Jacobs, A., Van Gerwen, V., Smouts, I., Pou-Serradell, A., Martin, J.J., Timmerman, V., and De Jonghe, P. (2004). SPTLC1 mutation in twin sisters with hereditary sensory neuropathy type I. *Neurology* **62**, 1001–1002.
- Wang, L., Zhou, Y., Liu, B., Huang, S., Hou, F., and Ge, J. (2007). Pro370Leu mutant myocilin disturbs the endoplasmic reticulum stress response and mitochondrial membrane potential in human trabecular meshwork cells. *Mol Vis* **13**, 618–625.

Address correspondence to:

Garth A. Nicholson, PhD
Northcott Neuroscience Laboratory
ANZAC Research Institute
University of Sydney
Hospital Road
Concord 2139
NSW
Australia

E-mail: garth.nicholson@sydney.edu.au

Simon J. Myers, PhD
Neuro-Cell Biology Laboratory
Molecular Medicine Research Group
University of Western Sydney
Narellan Road
Campbelltown 2560
NSW
Australia

E-mail: s.myers@uws.edu.au

Received for publication August 1, 2013; received in revised form February 21, 2014; accepted February 22, 2014.